https://doi.org/10.5194/essd-2026-103
Preprint. Discussion started: 1 April 2026
© Author(s) 2026. CC BY 4.0 License.

Open Access Earth System Science Data Discussions

Daily Human Thermal Index Dataset for India (HiTIC-India) at 1-km Spatial Resolution (2003–2020).

Subhransu Sekhar Gouda[a] , Saket Dubey[a]*,Vrinda Kankanala[a], Jasinta Gera[a], and Sukeerthi Bharatha[a]

[a]School of Infrastructure, Indian Institute of Technology, Bhubaneswar 752050, India

Corresponding author: Saket Dubey

Email id: saketdubey@iitbbs.ac.in

https://doi.org/10.5194/essd-2026-103
Preprint. Discussion started: 1 April 2026
© Author(s) 2026. CC BY 4.0 License.

Open Access Earth System Science Data Discussions

Abstract

Human exposure to extreme heat and cold poses increasing risks to public health, labour productivity, and urban sustainability, particularly in densely populated and climate-sensitive regions such as India. Human-perceived temperature (HPT) indices provide a more realistic measure of thermal stress than air temperature alone by integrating multiple meteorological factors. Here, we present the Human Thermal Index Collection for India (HiTIC-India), a high-resolution daily gridded dataset comprising twelve widely used HPT indices at 1 km spatial resolution for 2003–2020. The indices are initially derived from ERA5-based meteorological data and then downscaled using a Light Gradient Boosting Machine (LightGBM) framework. This downscaling incorporates satellite-derived land surface temperature, precipitable water vapour, population density, and topographic variables (slope, elevation and aspect) to generate spatially continuous predictions at 1 km resolution. Model valuation shows high prediction accuracy across all indices, with a mean root-mean-square error (RMSE) of 3.12 °C, a coefficient of determination (R^2) of 0.89, and a mean absolute error (MAE) of 2.39 °C. The resulting dataset significantly captures local-scale variability in heat and cold stress across India's diverse climatic and physiographic zones. HiTIC-India also supports numerous applications, including public health risk evaluation, urban heat exposure analysis, labour productivity assessment, and climate adaptation and mitigation planning. By providing consistent daily HPT datasets, HiTIC-India provides a comprehensive, high-resolution, and publicly accessible resource for climate–health research and evidence-based decision-making under warming climate.

Keywords: Covariates, ERA-5 datasets, Heatwaves and cold waves, Human-Perceived Temperature (HPT), India, Light Gradient Boosting Machine (LightGBM).

https://doi.org/10.5194/essd-2026-103
Preprint. Discussion started: 1 April 2026
© Author(s) 2026. CC BY 4.0 License.

Open Access Earth System Science Data Discussions

Introduction

Ongoing climate change is fundamentally reshaping the global climate system, leading to widespread impacts across agricultural productivity, public health, and economic stability (Burke et al., 2015; Vanos et al., 2020). These changes result from the increasing frequency and severity of extreme weather such as droughts, heatwaves, coldwaves, and heavy precipitation (Utep et al., 2014; Vicedo-Cabrera et al., 2021; Wang et al., 2020). Heatwaves and coldwaves are especially critical due to their direct and indirect impacts on human health, often triggering cascading hazards such as wildfires and substantial increases in temperature-related mortalities (Dunne et al., 2013; Kumar et al., 2025; Kumar and Mishra, 2020; Li et al., 2020; Mora et al., 2017; Yan et al., 2021). The historical record underscores the severe consequences of these thermal extremes, with the 2003 European and 2010 Russian heatwaves resulting in over 70,000 and 55,000 excess deaths, respectively (Barriopedro et al., 2011; Robine et al., 2008). While research attention has predominantly focused on extreme heat, growing evidence indicates that cold waves can be equally or even more lethal. Between 2000 and 2013, Madrid recorded nearly 900 deaths across 1,542 cold-wave events (López-Bueno et al., 2021), while in the United States, extreme cold accounted for approximately 63% of all weather-related fatalities from 2006 to 2010 (Berko et al., 2014). The above instances highlight the escalating societal risks posed by temperature extremes and highlight the need of high-resolution datasets to monitor human thermal stress.

In this context, HPT indices serve as essential parameters for measuring physiological stress induced by environmental conditions across diverse atmospheric conditions (Li et al., 2023, 2025; Di Napoli et al., 2018; Yan et al., 2021). Unlike assessments based solely on near-surface air temperature, HPT indices integrate multiple meteorological variables including air temperature, humidity, wind speed, and solar radiation to provide a more physiologically relevant characterization of human thermal stress (Cheng et al., 2019; Joubert et al., 2011; Zhang et al., 2013). Under hot and humid conditions, high moisture levels inhibit evaporative cooling through sweating, leading to the accumulation of heat in the human body and perceived temperatures that exceed actual air temperature (Chan and Yi, 2016; Kjellstrom et al., 2009; Willett and Sherwood, 2012). Conversely, under colder conditions, strong winds enhance convective heat loss from the body, resulting in lower perceived temperatures and substantially

https://doi.org/10.5194/essd-2026-103
Preprint. Discussion started: 1 April 2026
© Author(s) 2026. CC BY 4.0 License.

intensifying cold stress (Chan and Yi, 2016; Kjellstrom et al., 2009; Osczevski and Bluestein, 2005). These physiological responses explain why extreme HPT values are strongly associated with adverse health outcomes such as respiratory stress, reduced skin evaporation, and greater risks of illness and death among vulnerable populations (Barriopedro et al., 2011; Campbell et al., 2018; Robine et al., 2008). Despite their relevance, most existing HPT assessments rely on sparse meteorological station observations or coarse-resolution climate and reanalysis products, which are unable to capture the fine-scale spatial variability of human thermal stress. Therefore, developing high-resolution, temporally consistent HPT datasets is crucial for understanding climate–health research and improving assessments of population exposure to thermal extremes.

Over the past few decades, India has seen a notable rise in extreme weather events, posing escalating risks to public health. These risks are further amplified by the country's dense population, rapid urbanisation, and persistent socioeconomic inequalities (Oakes, 2009). Extreme thermal events, particularly heatwaves during the pre-monsoon and summer months (March–July) and cold waves in winter (December–February), now account for hundreds of deaths annually, with heat-related mortalities increasing by approximately 146% between 1967 and 2009 (Mazdiyasni et al., 2025; Ray et al., 2021). The catastrophic nature of thermal extremes in India is underscored by a series of high-impact events that directly correlate temperature surges with excess mortality. Major urban centres have recorded substantial spikes in death rates during intense heatwaves, including the May 2010 heatwave in Ahmedabad (Azhar et al., 2014), and prolonged high-temperature periods in Surat during 2014–2015 (Rathi et al., 2017). Similarly, in Varanasi, rising summer temperatures have been linked to a clear increase in overall mortality risk (Singh et al., 2019). Beyond heat, cold waves also impose considerable health and economic burdens across the country. Historical records from 1978 to 2014 indicate that hundreds of cold-wave events have claimed thousands of lives, with the highest casualties traditionally concentrated in northern states like Uttar Pradesh and Bihar (Malik et al., 2020). A particularly lethal cold wave in January 2003 alone resulted in nearly a thousand excess deaths (De et al., 2005). The impact of these climate extremes extends beyond public health to the region's economic and social fabric. Severe cold events have led to staggering financial losses in the agricultural sector, notably the

https://doi.org/10.5194/essd-2026-103
Preprint. Discussion started: 1 April 2026
© Author(s) 2026. CC BY 4.0 License.

Open Access Earth System Science Data Discussions

2006 cold event in Rajasthan, where crop damage reached devastating levels (Malik et al., 2020). Furthermore, thermal stress fundamentally disrupts daily livelihoods by compromising labour productivity. Surveys of the Indian labourers indicate that most outdoor and informal workers face hazardous levels of heat stress during summer months, yet a significant portion remains vulnerable to physiological thermal stress even during cooler periods (Venugopal et al., 2016). Despite these widespread impacts, available datasets are often coarse, underscoring the need for high-resolution HPT datasets to better understand and manage thermal stress at local and regional scales.

To address this gap, we present the HiTIC-India, a daily gridded dataset comprising 12 key HPT indices at a 1 km resolution covering the period 2003–2020. To our knowledge, this is the first dataset to offer such high spatial detail for the entire Indian subcontinent, significantly improving upon previously available coarser-resolution products (Yan et al., 2021). The dataset provides a scientific foundation for understanding spatial variability in thermal stress and is directly relevant to public health planning, occupational safety, urban development, and climate adaptation strategies.

Methods

This study includes twelve core HPT indices calculated using four meteorological variables: air temperature at 2 m height, relative humidity at 2 m height (RH), actual vapour pressure (Ea), and wind speed. These variables are obtained as daily gridded products from the ERA5 agro-meteorological indicators (0.1° × 0.1°) and the Copernicus Climate Change Service Climate Data Store (0.25° × 0.25°). All meteorological variables are harmonized to a common daily spatial resolution of 0.1° × 0.1°, after which twelve HPT indices including Indoor Apparent Temperature (ATin), Discomfort Index (DI), Effective Temperature (ET), Heat Index (HI), Humidex (HMI), Modified Discomfort Index (MDI), Net Effective Temperature (NET), Outdoor Shaded Apparent Temperature (ATout), Surface Air Temperature (SAT), Simplified Wet-Bulb Globe Temperature (SWBGT), Wet-Bulb Temperature (WBT), and Wind Chill Temperature (WCT) are calculated using standard formulations (Table 1).

To derive HPT indices at a finer spatial resolution of 1 km, we incorporated a set of gridded covariates available at 1 km resolution, including LST, population density, precipitable water vapour (PWV),

https://doi.org/10.5194/essd-2026-103
Preprint. Discussion started: 1 April 2026
© Author(s) 2026. CC BY 4.0 License.

elevation, slope, and aspect. Together, these covariates capture key surface, atmospheric, and topographic influences on near-surface thermal conditions. To maintain consistency with the coarse-resolution HPT indices, all covariates are first regridded and aggregated to a common 0.1° × 0.1° resolution. Pixel-wise values of the regridded covariates and their corresponding HPT indices are then extracted and combined to form a set of candidate samples for model development. These samples are randomly divided into training (80%) and testing (20%) subsets and used within the LightGBM framework. Model optimisation is performed via hyperparameter tuning using a five-fold cross-validation approach, systematically exploring combinations of hyperparameters controlling tree structure, learning rate, and boosting behaviour to identify the most suitable model configuration (A Ilemobayo et al., 2024). Hyperparameter optimisation is implemented using a grid search strategy, in which predefined parameter ranges are specified, and the model is iteratively trained and evaluated across all possible combinations to determine the most effective configuration (Ngoc et al., 2022). Then the trained LightGBM model is applied across spatially continuous covariate fields maintained at their native 1 km resolution. This step enables the generation of high-resolution (1 km) gridded datasets for all twelve HPT indices. Model performance is evaluated using standard statistical metrics, including the coefficient of determination (R^2), root-mean-square error (RMSE), and mean absolute error (MAE). An overview of the complete methodological workflow is shown in figure 1.

https://doi.org/10.5194/essd-2026-103
Preprint. Discussion started: 1 April 2026
© Author(s) 2026. CC BY 4.0 License.

Open Access Earth System Science Data Discussions

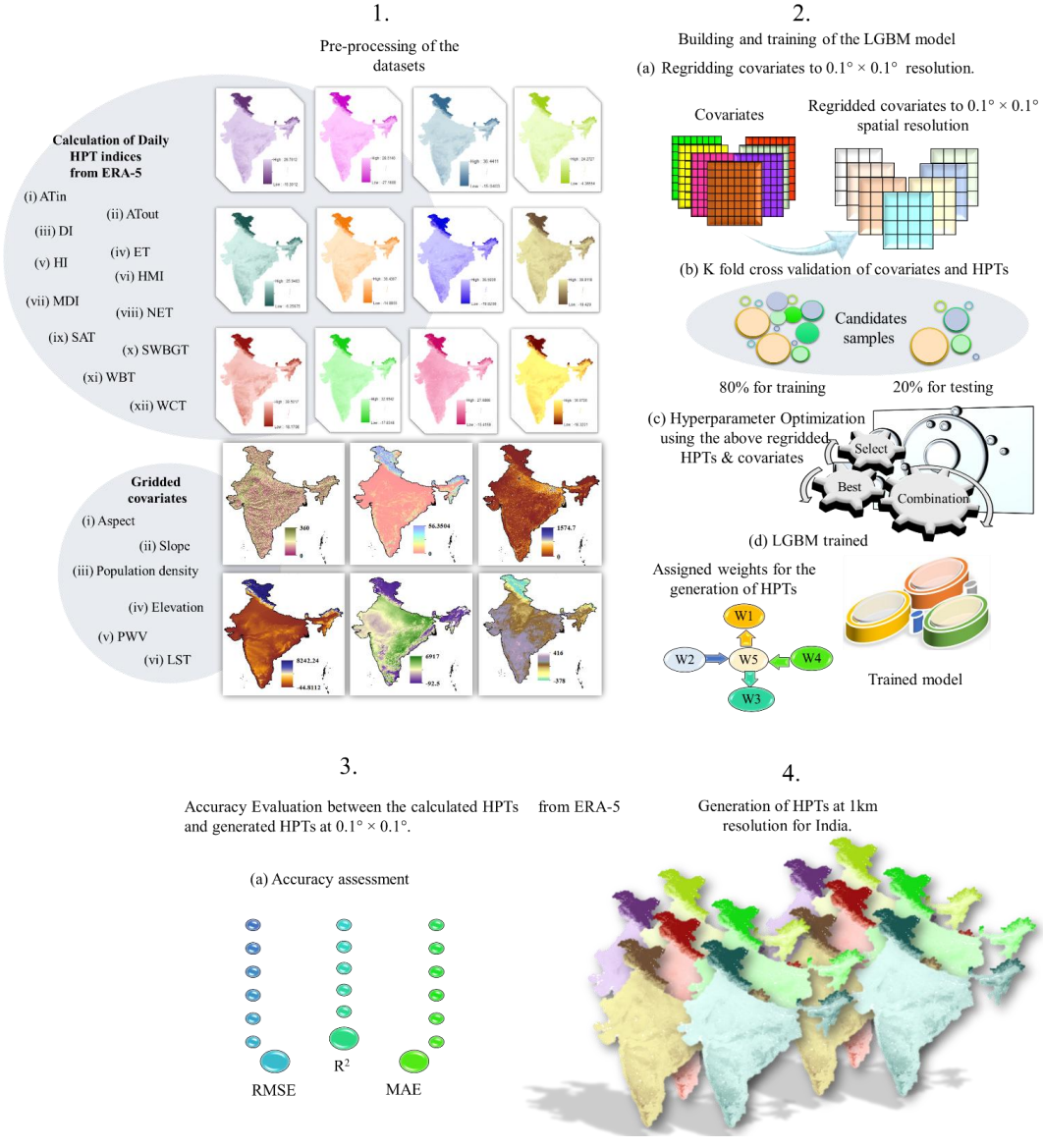

128

https://doi.org/10.5194/essd-2026-103
Preprint. Discussion started: 1 April 2026
© Author(s) 2026. CC BY 4.0 License.

Fig 1. Overview of the workflow used to generate the HiTIC-India dataset. The process includes (1) computation of twelve daily human-perceived temperature (HPT) indices from ERA5 data and obtaining gridded covariates, (2) training and optimisation of LightGBM model using regridded inputs at 0.1° × 0.1° resolution, (3) evaluation of model performance using RMSE, R^2, and MAE, and (4) generation of spatially continuous daily HPT datasets at 1 km resolution across India.

LightGBM

LightGBM is a highly efficient machine learning model, particularly suitable for gradient boosting tasks (Wang and Wang, 2020). A key feature of this model is its ability to handle large high-dimensional datasets and complex applications such as image classification. The model also employs a histogram-based learning approach, which groups continuous variables into discrete bins. This approach significantly accelerates model training and reduces memory usage compared with traditional gradient boosting methods, which enables it to manage extensive datasets while minimising both computational time and memory usage (Ke et al., 2017). Further, it exhibits remarkable accuracy and robustness, especially in environments where data is noisy and heterogeneous, making it particularly suitable for environmental and climate-related applications (Ma et al., 2022; Tian et al., 2021; Zhang et al., 2022a). Additionally, its flexible hyperparameter configuration allows the model to be customised to a wide range of data characteristics and modelling objectives (Cao et al., 2023; Chen, 2024; Shi and Zhang, 2023). Hence, it is one of the preferred models among various machine learning methods. Given its combination of efficiency, robustness, and flexibility, LightGBM is adopted in this study as the primary modelling framework for generating high-resolution HPT datasets.

Meteorological parameters and the role of HPT indices in assessing human thermal stress.

The meteorological variables (figure 2) play distinct roles in influencing human thermal stress: air temperature sets the baseline thermal environment, humidity and vapour pressure regulate evaporative cooling, and wind speed affects heat exchange between the human body and the surrounding air. By combining these variables, twelve core HPT indices are developed, representing different aspects of human thermal comfort and stress under varying atmospheric conditions (Li et al., 2023).

https://doi.org/10.5194/essd-2026-103
Preprint. Discussion started: 1 April 2026
© Author(s) 2026. CC BY 4.0 License.

Open Access Earth System Science Data Discussions

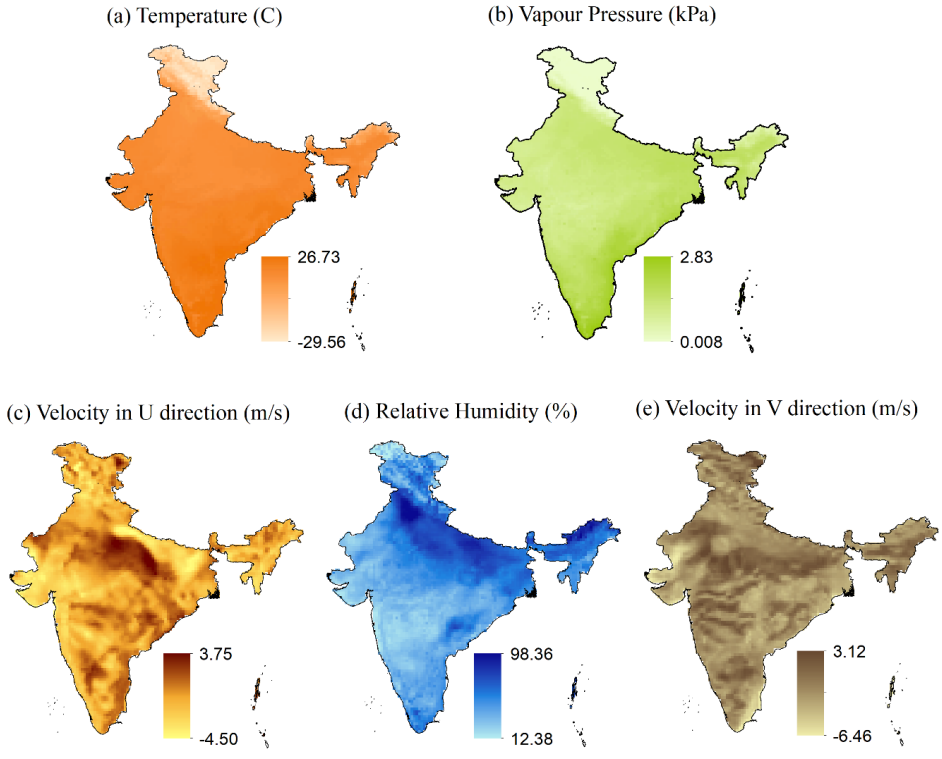

Fig 2. Spatial distribution of key meteorological parameters over India derived from the ERA 5 dataset. (a) Air temperature (°C), (b) actual vapour pressure (kPa), (c) wind velocity in the U (zonal) direction (m/s), (d) relative humidity (%), and (e) wind velocity in the V (meridional) direction (m/s). These parameters are used as input variables for calculating the HPTs.

The twelve indices in HiTIC-India are categorized based on their physiological relevance and the environmental variables they integrate. Apparent Temperature (AT)metrics, including Indoor (ATin) and Outdoor (ATout) variants, reflect the air temperature as perceived by the human body; ATin focuses on temperature and humidity, while ATout incorporates wind speed and solar radiation to assess outdoor exposure risks like cardiovascular strain (Epstein and Moran, 2006; Gagge et al., 1971). Heat Dissipation indices, such as the WBT and the SWBGT, measure the body's capacity for evaporative cooling. High values in these metrics indicate a decrease in ability to sweat, leading to severe risks of heat exhaustion or heatstroke (Stull, 2011; Willett and Sherwood, 2012). Operational indices like HI

https://doi.org/10.5194/essd-2026-103
Preprint. Discussion started: 1 April 2026
© Author(s) 2026. CC BY 4.0 License.

and HMI are widely used in public health and weather services for quantifying thermal discomfort. They merge temperature and humidity to define safety thresholds, with specific danger levels for heat cramps and heatstroke (Masterton and Richardson, 1981; Rothfusz et al., 1990; Steadman, 1979). Similarly, the DI and ET integrate moisture and wind speed to reflect heart rate and core temperature temperature (Epstein and Moran, 2006; Gagge et al., 1971). The MDI further serves as a reliable alternative to SWBGT in regions where field data are unavailable (Moran et al., 1998). Studies conducted in the USA, Egypt, and Israel showed a strong correlation between MDI and SWBGT (Moran et al., 1998). The NET provides a comprehensive assessment by balancing heat, moisture, and wind speed to represent overall thermal comfort across diverse climatic conditions (Houghton and Yaglo, 1923). Cold-related thermal stress is captured by the WCT, which accounts for accelerated heat loss from exposed skin under cold, windy conditions to assess risks of frostbite and hypothermia (Osczevski and Bluestein, 2005).

Table 1: Equations of the 12 HPTs used in the HiTIC-India Dataset. Each index integrates a combination of meteorological variables to reflect thermal stress under varying environmental conditions. These indices enable a more nuanced understanding of thermal discomfort across diverse climatic and topographic settings.

Name	**Human Thermal Index**	**Equation**
AT_{in}	Apparent Temperature (indoors)	$AT_{in} = -1.3 + 0.92 \times T + 2.2 \times Ea$
AT_{out}	Apparent Temperature	$AT_{out} = -2.7 + 1.04 \times T + 2 \times Ea - 0.65 \times V$

https://doi.org/10.5194/essd-2026-103
Preprint. Discussion started: 1 April 2026
© Author(s) 2026. CC BY 4.0 License.

	(outdoors, in the shade)	
DI	Discomfort Index	$DI = 0.5 \times WBT + 0.5 \times T$
ET	Effective Temperature	$ET = T - 0.4 \times (T - 10) \times (1 - 0.001 \times RH)$
HI	Heat Index	$HI = -8.784695 + 1.61139411 \times T - 2.338549 \times RH - 0.14611605 \times T \times RH - 1.2308094 \times 10^{-2} \times T^2 - 1.6424828 \times 10^{-2} \times RH^2 + 2.211732 \times 10^{-3} \times T^2 \times RH + 7.2546 \times 10^{-4} \times T \times RH^2 + 3.582 \times 10^{-6} \times T^2 \times RH^2$
HMI	Humidex	$HMI = T + 0.5555 \times (0.1 \times Ea - 10)$
MDI	Modified Discomfort Index	$MDI = 0.75 \times WBT + 0.38 \times T$
SAT	Surface Air Temperature	Air temperature at 2-meter height
SWBGT	Simplified Wetbulb Temperature	$SWGBT = 0.567 \times T + 0.0393 \times Ea + 3.94$
WBT	Web-bulb Temperature	$WBT = T \times \text{a tan}(0.151977 \times (RH + 8.313689)^{0.5}) + \text{a tan}(T + RH) - a\ tan(RH - 1.676331) + 0.00391838 \times RH^{\times 1.5} \times \text{a tan}(0.02301 \times RH) - 4.686035$
NET	Net Effective Temperature	$NET = 37 - \frac{37-T}{0.68-0.0014 \times RH + \frac{1}{1.76+1.4 \times V^{0.75}}} - 0.29 \times T \times (1 - 0.01 \times RH)$

https://doi.org/10.5194/essd-2026-103
Preprint. Discussion started: 1 April 2026
© Author(s) 2026. CC BY 4.0 License.

WCT	Wind Chill Temperature	$WCT = 13.12 + 0.6215 \times T - 11.37 \times (V \times 3.6)^{0.16} + 0.3965 \times T \times (V \times 3.6)^{0.16}$

Gridded covariates and their significance

The LST is included as a key covariate and is obtained from the Moderate Resolution Imaging Spectroradiometer (MODIS). To address cloud-induced data gaps, we used a globally consistent, gap-filled daily MODIS LST dataset at 1 km resolution (Zhang et al., 2022b) for the period 2003–2020. This dataset uses a two-stage spatiotemporal gap-filling framework that combines quality-controlled preprocessing with correlation-based and weighted-residual interpolation, ensuring spatial continuity and preserving temporal variability. Their cross-validation indicates high accuracy, with root mean square errors (RMSE) of 1.88 °C for daytime and 1.33 °C for nighttime LST (Zhang et al., 2022b). Furthermore, the population density datasets are obtained from the WorldPop project at 1 km spatial resolution and daily temporal resolution. It is an important indicator of anthropogenic influence on near-surface thermal conditions, as densely populated urban areas often experience higher temperatures relative to surrounding rural areas due to human activities such as transportation, industrial processes, and energy use (Gaughan et al., 2013). In addition, PWV, which represents the total water vapour in the atmosphere that can potentially form precipitation, is also included in the analysis to account for humidity-related effects on thermal stress (Lyapustin et al., 2022). Higher PWV increases humidity, reducing sweat evaporation and intensifying heat discomfort. Since HPTs depend on both air temperature and humidity, PWV directly influences heat stress. In this study, a global daily PWV dataset at 1 km resolution is incorporated to capture fluctuations in atmospheric humidity (Shiu et al., 2009; Society, 2022; Tian et al., 2022). Topographic factors such as elevation, slope, and aspect are derived from the Multi-Error-Removed Improved-Terrain (MERIT) Digital Elevation Model (DEM). The MERIT DEM corrects common errors in standard DEMs, such as stripe noise, speckle noise, and tree-height bias, thereby improving accuracy. These corrections are especially important in flat regions,

https://doi.org/10.5194/essd-2026-103
Preprint. Discussion started: 1 April 2026
© Author(s) 2026. CC BY 4.0 License.

where traditional DEMs often create artificial gradients (Yamazaki et al., 2017). The covariates used in this study are illustrated in figure 3.

.

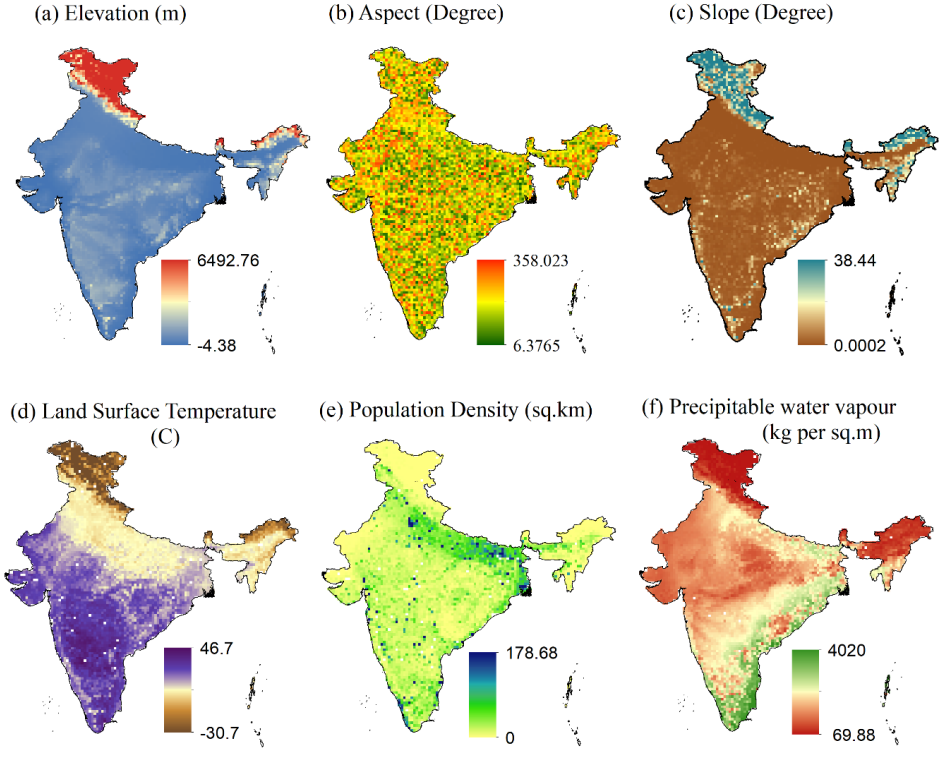

Fig 3. Spatial distribution of key covariates across India used in the study: (a) Elevation (m), (b) Aspect (degree), (c) Slope (degree), (d) Land Surface Temperature (°C), (e) Population Density (per sq. km), and (f) Precipitable Water Vapour (kg per sq. m).

Accuracy Evaluation

The model's prediction accuracy is evaluated using three statistical metrics. The statistical metrics include Root Mean Square Error (RMSE), the determination coefficient (R^2), and the mean absolute error (MAE). The equations for the following metrics are given in Equations (1), (2), and (3).

$$RMSE = \sqrt{\frac{\sum_{i=1}^{n}(x_{pi}-x)^2}{n}} \quad (1)$$

https://doi.org/10.5194/essd-2026-103
Preprint. Discussion started: 1 April 2026
© Author(s) 2026. CC BY 4.0 License.

$$R^2 = 1 - \frac{\sum_{i=1}^{n}(x_{oi}-x_{pi})^2}{\sum_{i=1}^{n}(x_{pi}-x)^2} \quad (2)$$

$$MAE = \frac{1}{n}(x_{oi} - x_{pi}) \quad (3)$$

Where n represents the total number of observations, while x_{oi} and x_{pi} are the observed and predicted values, respectively.

Results

The LightGBM models perform well across all twelve HPT indices at the ERA5 grid resolution. The validation results show that the models capture most of the day-to-day variability, with R^2 values ranging from 0.846 to 0.915. Prediction errors are generally low, with MAE ranging from 1.35 °C to 2.87 °C and RMSE between 1.75 °C and 3.75 °C. The best performance is obtained for indices such as ET, SWBGT, SAT, and HMI, which achieve higher R^2 values and lower errors. Indices that account for wind effects, such as WBT and NET, exhibit higher uncertainty but show reliable performance, with most R^2 values above 0.88 and similar error levels (figure 4). Overall, the results indicate that the modelling approach provides accurate and stable datasets of daily HPT at 1-km resolution across India.

https://doi.org/10.5194/essd-2026-103
Preprint. Discussion started: 1 April 2026
© Author(s) 2026. CC BY 4.0 License.

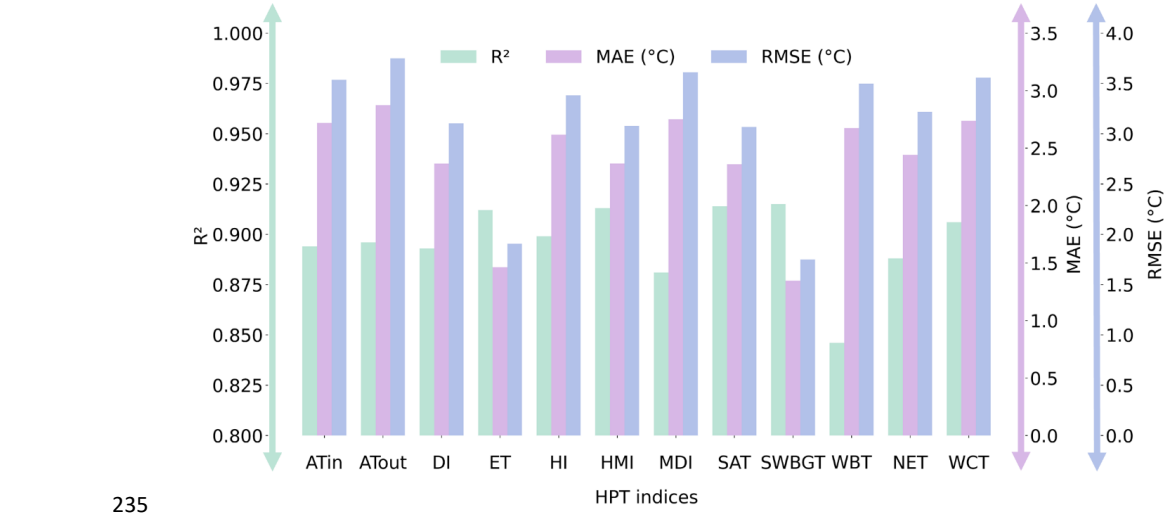

Fig 4: Comparison of model performance using three statistical metrics: Determination coefficient (R^2), Mean Absolute Error (MAE), and Root Mean Square Error (RMSE) for twelve HPT indices.

To evaluate the overall performance of the model across all twelve HPT indices, a Taylor diagram is used to compare the predicted HPT values with the corresponding ERA5-derived HPT data (figure. 5). The results show that the modelled indices are closely clustered around the reference point (denoted by the black star), indicating a strong agreement between the model predictions and the ERA5-based HPT values. All indices exhibit high correlation coefficients, generally exceeding 0.92, and closely matched standard deviations, indicating that the model effectively reproduces both the temporal variability and the magnitude of the ERA5-derived HPT data. These results confirm the robustness of the LightGBM-based approach and support its suitability for generating spatially consistent, high-resolution human thermal stress products.

https://doi.org/10.5194/essd-2026-103
Preprint. Discussion started: 1 April 2026
© Author(s) 2026. CC BY 4.0 License.

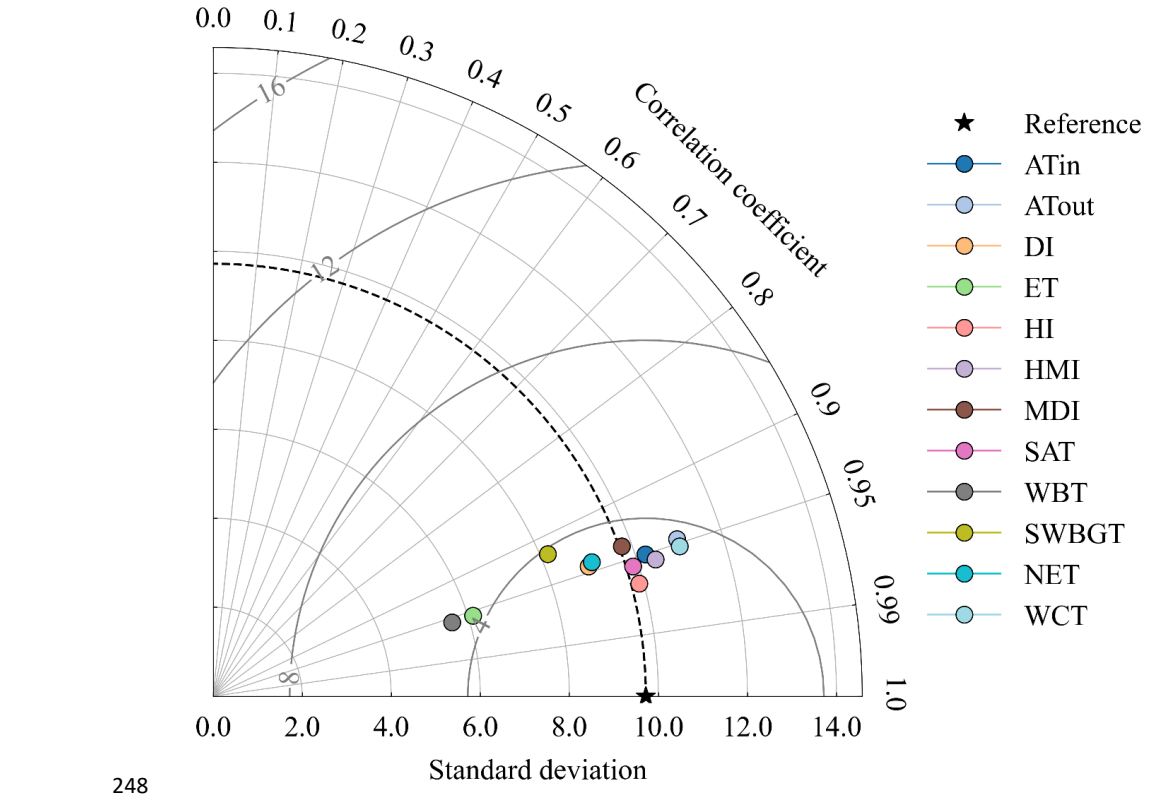

Fig 5: Taylor's diagram for the 12 HPTs.

The figure 6 depicts the year-wise performance of the LightGBM models for all twelve HPT indices from 2003 to 2020 using RMSE, R^2, and MAE. Across the study period, the predicted indices show consistent agreement with the corresponding ERA5-derived HPT values. RMSE values (figure 6a) generally range between about 1.7 and 3.9 °C, with lower errors for indices such as ET and SWBGT, and relatively higher values for ATout, MDI, and WCT. The coefficients of determination (R^2; figure 6b) remain high in all years, typically between 0.84 and 0.92, indicating that the temporal variability in ERA5-based HPTs is well captured by the model. Indices including ET, SWBGT, SAT, and HMI consistently exhibit higher R^2 values, whereas WBT shows lower R^2 values. MAE values (figure 6c) largely fall within the range of about 1.3 to 3.0 °C, again showing lower errors for ET and SWBGT and higher errors for ATout and WCT.

https://doi.org/10.5194/essd-2026-103
Preprint. Discussion started: 1 April 2026
© Author(s) 2026. CC BY 4.0 License.

Open Access Earth System Science Data Discussions

260

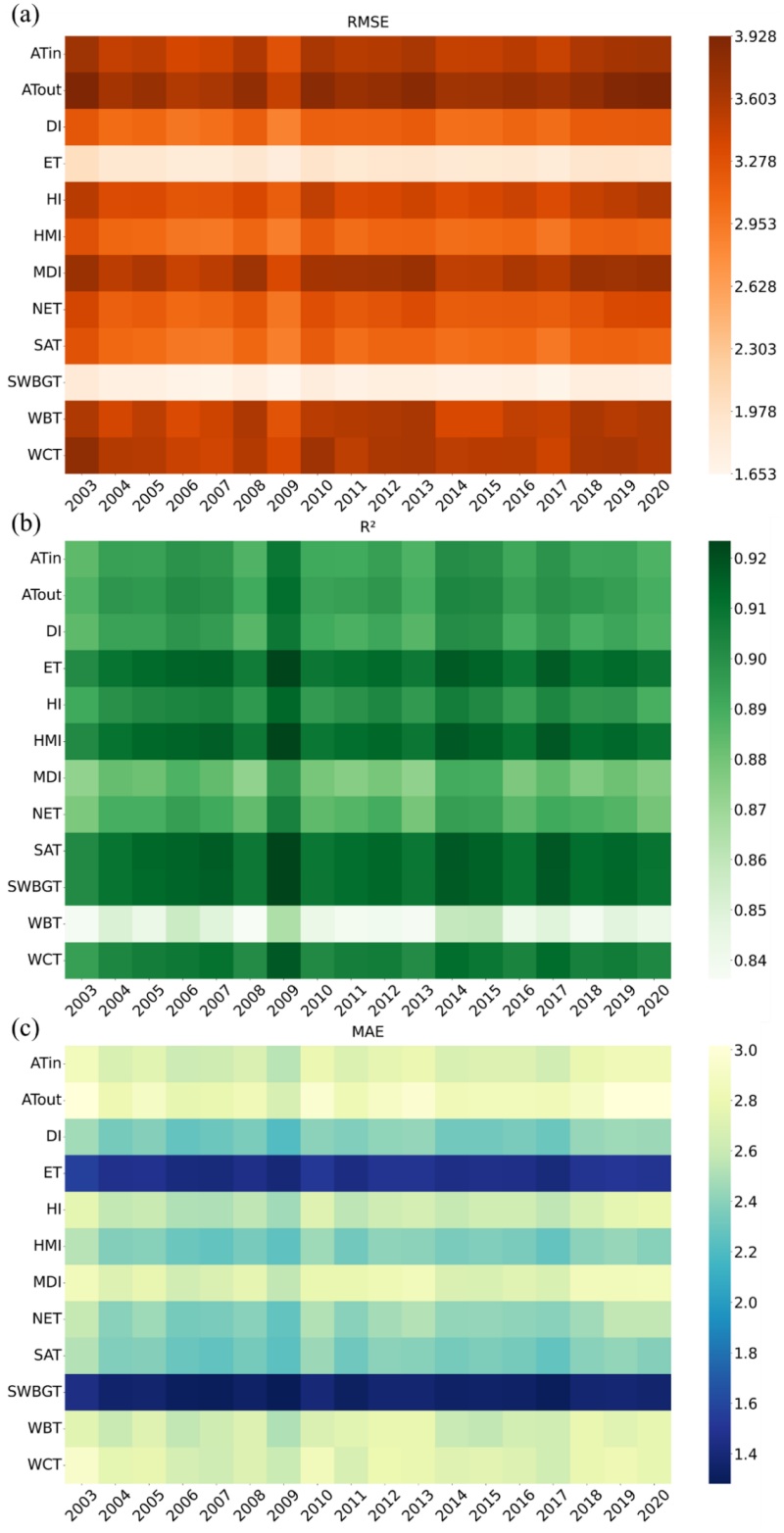

https://doi.org/10.5194/essd-2026-103
Preprint. Discussion started: 1 April 2026
© Author(s) 2026. CC BY 4.0 License.

Fig 6: Heatmap for the 12 indices for different years: (a) RMSE heatmap; (b) R^2 heatmap; (c) MAE heatmap.

The plots of predicted versus observed values for each of the twelve indices on the test dataset show strong agreement across all metrics. Each subplot shows a well-aligned distribution along the diagonal, indicating that the model's predictions closely match the observed values (figure 7). The closer clustering of points around the diagonal for indices suggests high model accuracy with minimal deviation.

https://doi.org/10.5194/essd-2026-103
Preprint. Discussion started: 1 April 2026
© Author(s) 2026. CC BY 4.0 License.

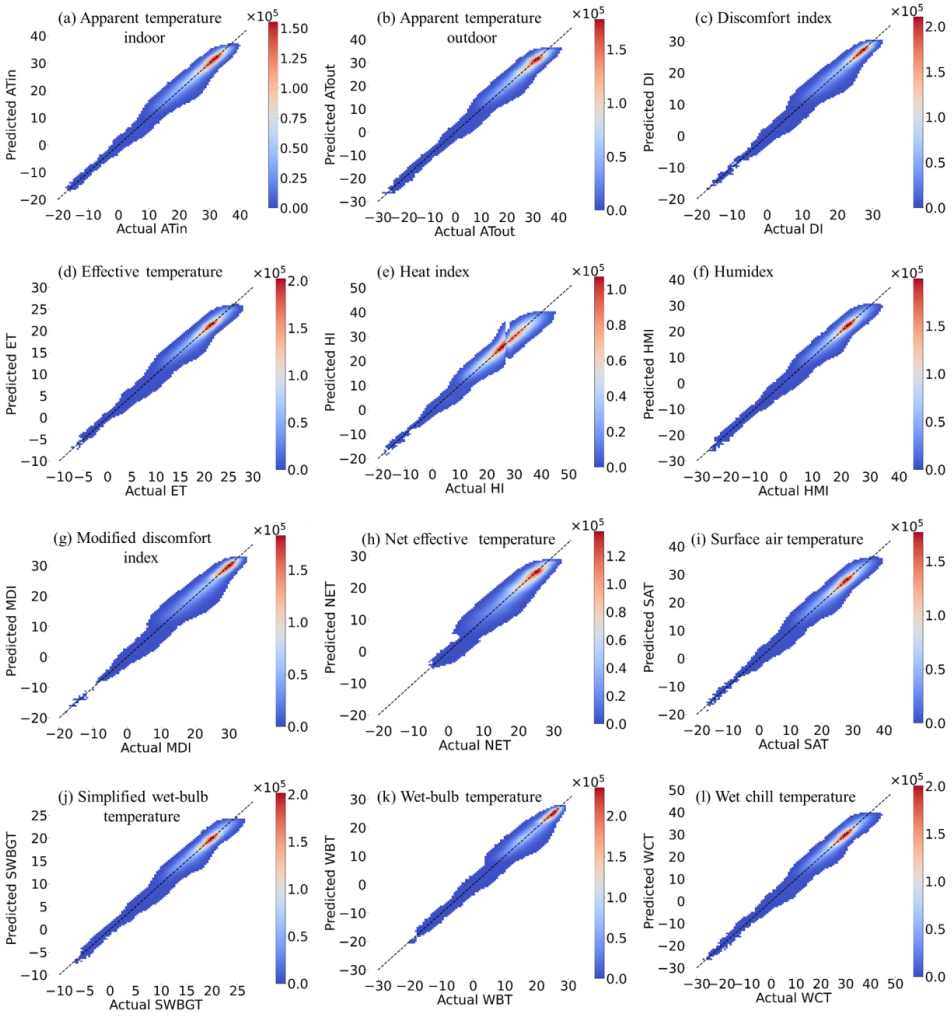

Fig. 7: Density plots showing the comparison between actual and predicted values of twelve HPTs. Each subplot corresponds to a specific HPT. The colour bar indicates the density of data points, with warmer colours representing higher concentrations.

Comparison of the HTI indices during a summer and winter day:

The spatial patterns of the HPTs show clear contrasts between summer and winter thermal environments across the Indian subcontinent. On 17 May 2015, heat-related indices such as ET, HI, HMI, SAT, SWBGT, and NET exhibit higher values over large parts of central, northern, and eastern India, indicating widespread heat stress (figure 8). In contrast, lower values are observed in high-elevation

https://doi.org/10.5194/essd-2026-103
Preprint. Discussion started: 1 April 2026
© Author(s) 2026. CC BY 4.0 License.

regions, particularly across the Himalayas, where complex topography maintains significantly lower perceived temperatures.

Conversely, on 20 December 2015, cold-related indices such as WBT, WCT, and SWBGT indicate higher cold stress levels across northern and north-western India, with notably low values over the Indo-Gangetic Plain and the Himalayan region (figure 9). Southern and coastal regions show relatively moderate conditions across most indices. These examples highlight the strong seasonal variations of the HPTs and their ability to reflect regional differences in human thermal stress under varying atmospheric conditions.

https://doi.org/10.5194/essd-2026-103
Preprint. Discussion started: 1 April 2026
© Author(s) 2026. CC BY 4.0 License.

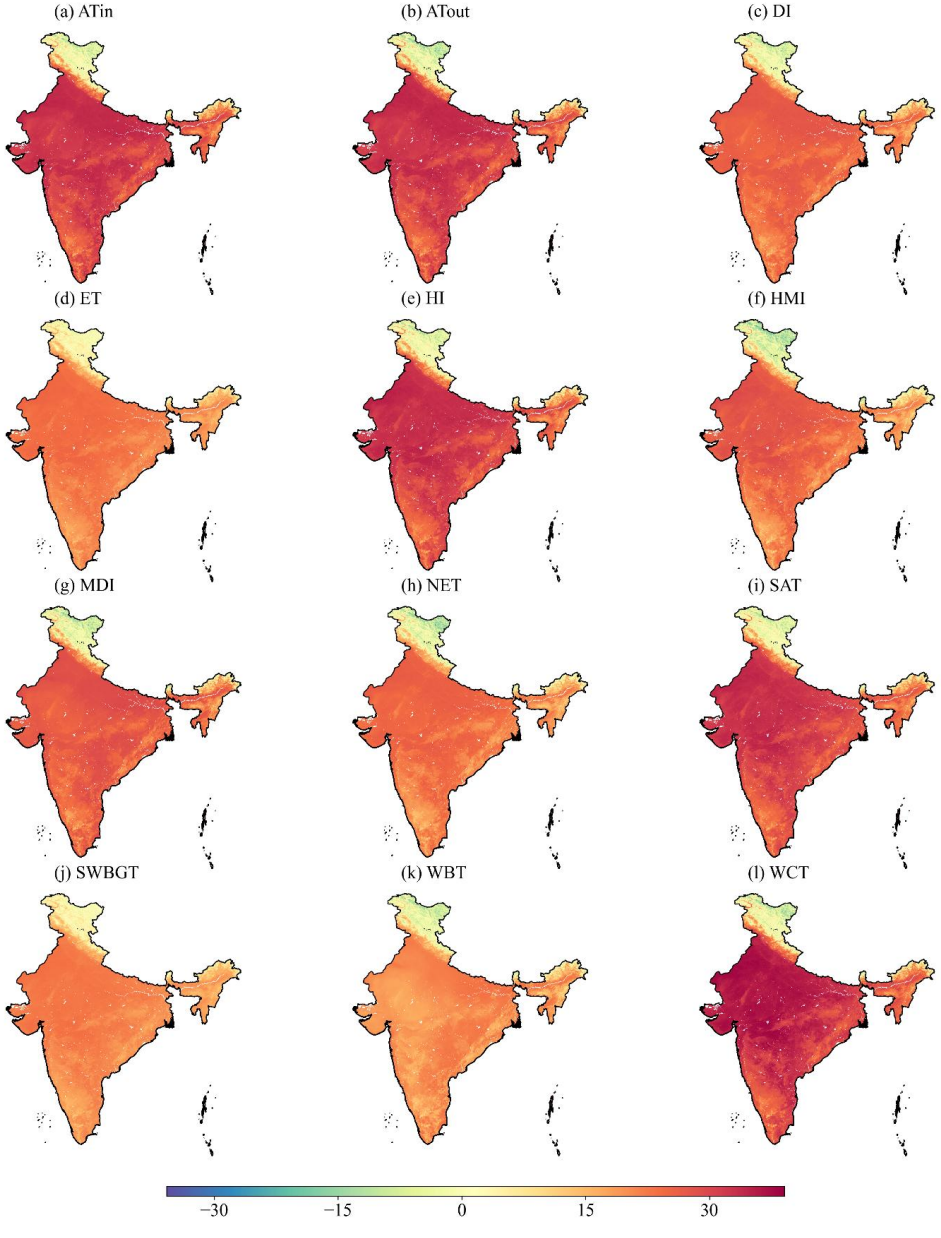

286

287 **Fig. 8: Spatial variation of 12 HPT indices at 1 km spatial resolution on 17 May 2015**. The maps
288 demonstrate the dataset's ability to identify localised heat stress hotspots across diverse geographic
289 regions.

https://doi.org/10.5194/essd-2026-103
Preprint. Discussion started: 1 April 2026
© Author(s) 2026. CC BY 4.0 License.

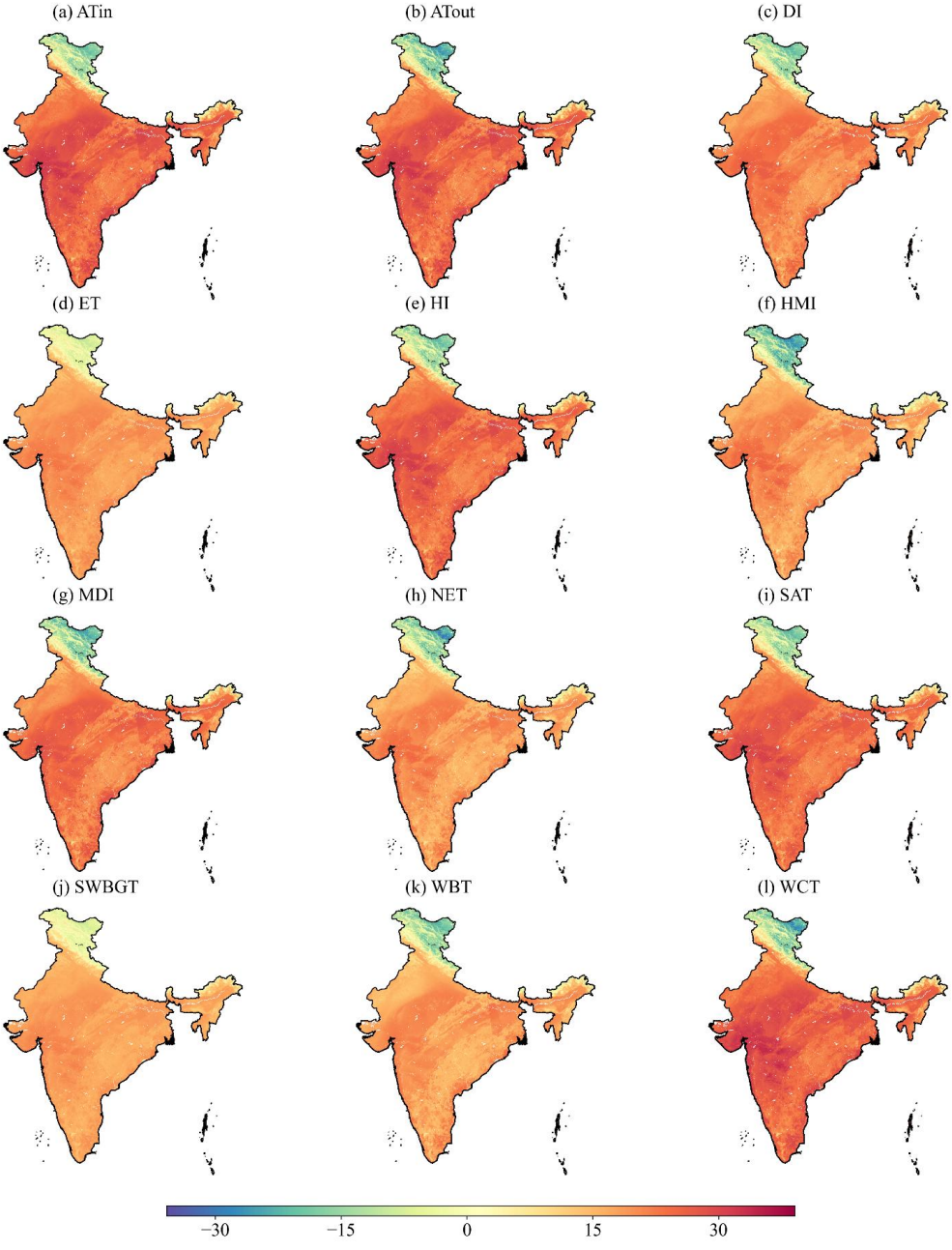

290

291 **Fig. 9: Spatial variation of 12 HPT indices at 1 km spatial resolution on 20 December 2015**. The
292 maps demonstrate the dataset's ability to identify localised cold stress hotspots across diverse
293 geographic regions.

https://doi.org/10.5194/essd-2026-103
Preprint. Discussion started: 1 April 2026
© Author(s) 2026. CC BY 4.0 License.

Conclusion

This study presents HiTIC-India, a high-resolution (1 km) gridded dataset of twelve HPT indices spanning 2003–2020. By integrating ERA5 reanalysis with satellite-derived and topographic covariates through a LightGBM framework, we have generated a spatially consistent record of thermal conditions across India. The model shows high prediction accuracy across all indices, ensuring the dataset is a dependable proxy for station-based observations in regions with sparse monitoring. HiTIC-India addresses the limitations of previous coarse-resolution products by capturing localised thermal extremes that are vital for public health and urban planning. By offering both daily and monthly outputs, this dataset supports a broad range of applications—from exploring long-term climate-health relationships and labour productivity losses to guiding local adaptation strategies. As a publicly accessible resource, HiTIC-India provides the high-resolution data needed to manage thermal risks in one of the world's most climate-vulnerable and densely populated areas.

Acknowledgement

The authors gratefully acknowledge the ERA5 agro-meteorological indicators (0.1° × 0.1°) and the ERA5 reanalysis datasets (Copernicus Climate Change Service Climate Data Store) for providing meteorological datasets. The research is conducted with the support of computational resources and infrastructure provided by the Indian Institute of Technology Bhubaneswar, India.

Authors contribution

Subhransu Sekhar Gouda: Conceptualisation, Data curation, Methodology, Visualisation, writing – original draft, Writing – review & editing.

Saket Dubey: Conceptualisation, Data curation, Supervision, Visualisation, Writing – review & editing.

VR: Data curation, Methodology and Visualisation, Writing – review & editing.

JG: Methodology and Visualisation, Writing – review & editing.

Sukeerti: Methodology and Visualisation, Writing – review & editing.

https://doi.org/10.5194/essd-2026-103
Preprint. Discussion started: 1 April 2026
© Author(s) 2026. CC BY 4.0 License.

Open Access Earth System Science Data Discussions

Data availability statement

Due to repository storage limitations, we provide monthly mean datasets for all twelve human-perceived temperature (HPT) indices for the period 2003–2020 via Zenodo (https://doi.org/10.5281/zenodo.18510627) (Gouda et al., 2026). The monthly products, which together occupy approximately 24 GB, are distributed in NetCDF (.nc) format and follow a consistent naming convention of the form **HPTindex**_monthly_mean_2003_2020.nc (for example, ATin_monthly_mean_2003_2020.nc, ET_monthly_mean_2003_2020.nc, and corresponding files for the remaining indices). Each file contains gridded monthly mean values at 1 km spatial resolution covering the full study region. The daily HPT predictions at 1 km resolution are substantially larger in size (7 TB) and therefore cannot be hosted in the public archive; however, a limited set of representative daily files is provided in the Zenodo record using the naming convention. Predicted_Year_**HPTindex**_Day_DOY.nc (for example, Predicted_2003_ATin_Day_001.nc). The complete daily HPT datasets will be made publicly available through the ISRO–NICES data portal prior to publication and, in the interim, are available from the authors upon reasonable request. The land surface temperature dataset at 1 km spatial resolution was obtained from https://doi.org/10.25380/iastate.c.5078492 (Zhang et al., 2022b). The population density dataset was accessed from the WorldPop repository via Google Earth Engine: https://developers.google.com/earth-engine/datasets/catalog/WorldPop_GP_100m_pop(Gaughan et al., 2013). Elevation, slope, and aspect layers were derived from the MERIT DEM dataset available at (Yamazaki et al., 2017). Precipitable water vapour (PWV) data at 1 km daily resolution were obtained from the MODIS MCD19A2 product is https://developers.google.com/earth-engine/datasets/catalog/MODIS_061_MCD19A2_GRANULES#dois (Lyapustin et al., 2022). The meteorological variables are obtained from https://cds.climate.copernicus.eu/datasets/sis-agrometeorological-indicators?tab=overview.
and https://cds.climate.copernicus.eu/datasets/reanalysis-era5-single-levels?tab=download

https://doi.org/10.5194/essd-2026-103
Preprint. Discussion started: 1 April 2026
© Author(s) 2026. CC BY 4.0 License.

References

A Ilemobayo, J., Durodola, O., Alade, O., J Awotunde, O., T Olanrewaju, A., Falana, O., Ogungbire, A., Osinuga, A., Ogunbiyi, D., Ifeanyi, A., E Odezuligbo, I., and E Edu, O.: Hyperparameter Tuning in Machine Learning: A Comprehensive Review, Journal of Engineering Research and Reports, 26, 388–395, https://doi.org/10.9734/jerr/2024/v26i61188, 2024.

Azhar, G. S., Mavalankar, D., Nori-Sarma, A., Rajiva, A., Dutta, P., Jaiswal, A., Sheffield, P., Knowlton, K., and Hess, J. J.: Heat-Related Mortality in India: Excess All-Cause Mortality Associated with the 2010 Ahmedabad Heat Wave, PLoS One, 9, e91831, 2014.

Barriopedro, D., Fischer, E. M., Luterbacher, J., Trigo, R. M., and García-Herrera, R.: The Hot Summer of 2010 : Map of Europe, Science (1979)., 332, 220–224, 2011.

Berko, J., Ingram, D. D., Saha, S., and Parker, J. D.: Deaths attributed to heat, cold, and other weather events in the United States, 2006-2010., Natl. Health Stat. Report., 1–15, 2014.

Burke, M., Hsiang, S. M., and Miguel, E.: Global non-linear effect of temperature on economic production, Nature, 527, 235–239, https://doi.org/10.1038/nature15725, 2015.

Campbell, S., Remenyi, T. A., White, C. J., and Johnston, F. H.: Heatwave and health impact research: A global review, Health Place, 53, 210–218, https://doi.org/10.1016/j.healthplace.2018.08.017, 2018.

Cao, Q., Wu, Y., Yang, J., and Yin, J.: Greenhouse Temperature Prediction Based on Time-Series Features and LightGBM, Applied Sciences (Switzerland), 13, https://doi.org/10.3390/app13031610, 2023.

Chan, Albert P C and Yi, Wen: Heat stress and its impacts on occupational health and performance, Indoor and Built Environment, 25, 3–5, https://doi.org/10.1177/1420326X15622724, 2016.

Chen, J.: LightGBM Model for Detecting Fraud in Online Financial Transactions, Highlights in Science, Engineering and Technology, 93, 363–371, https://doi.org/10.54097/xw0bng93, 2024.

Cheng, J., Xu, Z., Bambrick, H., Su, H., Tong, S., and Hu, W.: Impacts of exposure to ambient temperature on burden of disease: a systematic review of epidemiological evidence, Int. J. Biometeorol., 63, 1099–1115, https://doi.org/10.1007/s00484-019-01716-y, 2019.

De, U. S., Dube, R. K., and Rao, G. S. P.: Extreme Weather Events over India in the last 100 years, J. Ind. Geophys. Union, 9, 173–187, 2005.

Dunne, J. P., Stouffer, R. J., and John, J. G.: Reductions in labour capacity from heat stress under climate warming, Nat. Clim. Chang., 3, 563–566, https://doi.org/10.1038/nclimate1827, 2013.

Epstein, Y. and Moran, D.: Thermal Comfort and the Heat Stress Indices, Ind. Health, 44, 388–398, https://doi.org/10.2486/indhealth.44.388, 2006.

Gagge, A. P., Stolwijk, J. A. J., and Nishi, Y.: An effective temperature scale based on a simple model of human physiological regulatory response, ASHRAE Trans., 77, 247–262, 1971.

Gaughan, A. E., Stevens, F. R., Linard, C., Jia, P., and Tatem, A. J.: High Resolution Population Distribution Maps for Southeast Asia in 2010 and 2015, PLoS One, 8, https://doi.org/10.1371/journal.pone.0055882, 2013.

Gouda, S. S., Dubey, S., Kankanala, V., Gera, J., and Bharatha, S.: Daily Human Thermal Index Dataset for India (HiTIC-India) at 1-km Spatial Resolution (2003–2020)., https://doi.org/18510627, 2026.

https://doi.org/10.5194/essd-2026-103
Preprint. Discussion started: 1 April 2026
© Author(s) 2026. CC BY 4.0 License.

383 Houghton, F. C. and Yaglo, C. P.: Determining equal comfort lines, Journal of the American Society of
384 Heating and Ventilating Engineers, 29, 165–176, 1923.

385 Joubert, D., Thomsen, J., and Harrison, O.: Safety in the Heat: A Comprehensive Program for
386 Prevention of Heat Illness Among Workers in Abu Dhabi, United Arab Emirates, Am. J. Public Health,
387 101, 395–398, https://doi.org/10.2105/AJPH.2009.189563, 2011.

388 Ke, G., Meng, Q., Finley, T., Wang, T., Chen, W., Ma, W., Ye, Q., and Liu, T.-Y.: LightGBM: A Highly
389 Efficient Gradient Boosting Decision Tree, 2017.

390 Kjellstrom, T., Holmer, I., and Lemke, B.: Workplace heat stress, health and productivity – an increasing
391 challenge for low and middle-income countries during climate change, Glob. Health Action, 2, 2047,
392 https://doi.org/10.3402/gha.v2i0.2047, 2009.

393 Kumar, R. and Mishra, V.: Increase in Population Exposure Due to Dry and Wet Extremes in India
394 Under a Warming Climate, Earths Future, 8, https://doi.org/10.1029/2020EF001731, 2020.

395 Kumar, R., Gopikrishnan, G. S., and Kuttippurath, J.: Rapid changes in warm and cold extremes in
396 recent decades and their future projections for India, J. Environ. Manage., 387, 125832,
397 https://doi.org/https://doi.org/10.1016/j.jenvman.2025.125832, 2025.

398 Li, D., Yuan, J., and Kopp, R. E.: Escalating global exposure to compound heat-humidity extremes with
399 warming, Environmental Research Letters, 15, 64003, https://doi.org/10.1088/1748-9326/ab7d04,
400 2020.

401 Li, X., Luo, M., Zhao, Y., Zhang, H., Ge, E., Huang, Z., Wu, S., Wang, P., Wang, X., and Tang, Y.: A
402 daily high-resolution (1 km) human thermal index collection over the North China Plain from 2003 to
403 2020, Sci. Data, 10, 1–14, https://doi.org/10.1038/s41597-023-02535-y, 2023.

404 Li, X., Luo, M., Li, J., Wu, S., Zhang, H., Huang, Z., Wang, Q., Cao, W., Tang, Y., and Wang, X.:
405 Human-perceived temperature changes linked to local climate zones under extreme hot and cold
406 weathers: A study in the North China Plain, Sustain. Cities Soc., 121, 106201,
407 https://doi.org/10.1016/j.scs.2025.106201, 2025.

408 López-Bueno, J., Navas-Martin, M., Díaz, J., Miron, I., Luna, M. Y., Sanchez Martinez, G., Culqui
409 Lévano, D., and Linares, C.: The Effect of Cold Waves on Mortality in Urban and Rural Areas of
410 Madrid, Environ. Sci. Eur., 33, https://doi.org/10.1186/s12302-021-00512-z, 2021.

411 Lyapustin, A., Processes, Y. W.-N. E. L., and 2022, U.: MODIS/Terra+ aqua land aerosol optical depth
412 daily L2G global 1km SIN grid V061, ui.adsabs.harvard.edu,
413 https://doi.org/10.5067/MODIS/MCD19A2.061+(2022), 2022.

414 Ma, J., Zhang, R., Xu, J., and Yu, Z.: MERRA-2 PM2.5 mass concentration reconstruction in China
415 mainland based on LightGBM machine learning, Science of The Total Environment, 827, 154363,
416 https://doi.org/10.1016/j.scitotenv.2022.154363, 2022.

417 Malik, P., Bhardwaj, P., and Singh, O.: Distribution of cold wave mortalities over India: 1978–2014,
418 International Journal of Disaster Risk Reduction, 51, 101841,
419 https://doi.org/https://doi.org/10.1016/j.ijdrr.2020.101841, 2020.

420 Masterton, J. and Richardson, F.: Humidex: a method of quantifying human discomfort due to excessive
421 heat and humidity., https://doi.org/10.5555/19802408434, 1981.

422 Mazdiyasni, O., AghaKouchak, A., Davis, S. J., Madadgar, S., Mehran, A., Ragno, E., Sadegh, M.,
423 Sengupta, A., Ghosh, S., Dhanya, C. T., and Niknejad, M.: Increasing probability of mortality during
424 Indian heat waves, Sci. Adv., 3, e1700066, https://doi.org/10.1126/sciadv.1700066, 2025.

https://doi.org/10.5194/essd-2026-103
Preprint. Discussion started: 1 April 2026
© Author(s) 2026. CC BY 4.0 License.

Mora, C., Dousset, B., Caldwell, I. R., Powell, F. E., Geronimo, R. C., Bielecki, C. R., Counsell, C. W. W., Dietrich, B. S., Johnston, E. T., Louis, L. V., Lucas, M. P., Mckenzie, M. M., Shea, A. G., Tseng, H., Giambelluca, T. W., Leon, L. R., Hawkins, E., and Trauernicht, C.: Global risk of deadly heat, Nat. Clim. Chang., 7, 501–506, https://doi.org/10.1038/nclimate3322, 2017.

Moran, D. S., Shapiro, Y. A., Moran"', D. S., Shapiro', Y., Epstein', Y., Matthew', W., and Pandolfi, K. B.: A modified discomfort index (MDI) as an alternative to the wet bulb globe temperature (WBGT), Environmental Ergonomics VIII, Hodgdon JA, Heaney JH, Buono MJ (Eds), 77–80, 1998.

Di Napoli, C., Pappenberger, F., and Cloke, H. L.: Assessing heat-related health risk in Europe via the Universal Thermal Climate Index (UTCI), Int. J. Biometeorol., 62, 1155–1165, https://doi.org/10.1007/s00484-018-1518-2, 2018.

Ngoc, T. T., Dai, L. Van, and Minh, L. B.: Effects of Data Standardization on Hyperparameter Optimization with the Grid Search Algorithm Based on Deep Learning: A Case Study of Electric Load Forecasting, Advances in Technology Innovation, 7, 258–269, https://doi.org/10.46604/aiti.2022.9227, 2022.

Oakes, T.: Asia, V1-214-V1-219 pp., https://doi.org/10.1016/B978-008044910-4.00250-9, 2009.

Osczevski, R. and Bluestein, M.: The new wind chill equivalent temperature chart, AMERICAN METEOROLOGICAL SOCIETY, 86, 1453–1458, https://doi.org/10.1175/BAMS-86-10-1453, 2005.

Rathi, S. K., Desai, V. K., Jariwala, P., Desai, H., Naik, A., and Joseph, A.: Summer Temperature and Spatial Variability of all-Cause Mortality in Surat City, India, Indian Journal of Community Medicine, 42, 2017.

Ray, K., Giri, R. K., Ray, S. S., Dimri, A. P., and Rajeevan, M.: An assessment of long-term changes in mortalities due to extreme weather events in India: A study of 50 years' data, 1970–2019, Weather Clim. Extrem., 32, 100315, https://doi.org/https://doi.org/10.1016/j.wace.2021.100315, 2021.

Robine, J. M., Cheung, S. L. K., Le Roy, S., Van Oyen, H., Griffiths, C., Michel, J. P., and Herrmann, F. R.: Death toll exceeded 70,000 in Europe during the summer of 2003, C. R. Biol., 331, 171–178, https://doi.org/10.1016/j.crvi.2007.12.001, 2008.

Rothfusz, Headquarters, L. P. &, and R, N. S.: The heat index equation (or, more than you ever wanted to know about heat index), Fort Worth, Texas: National Oceanic and Atmospheric Administration, National Weather Service, Ofce of Meteorology, 9023, 640, 1990.

Shi, C. and Zhang, F.: A Forest Fire Susceptibility Modeling Approach Based on Integration Machine Learning Algorithm, Forests, 14, 1–16, https://doi.org/10.3390/f14071506, 2023.

Shiu, C. J., Liu, S. C., and Chen, J. P.: Diurnally asymmetric trends of temperature, humidity, and precipitation in Taiwan, J. Clim., 22, 5635–5649, https://doi.org/10.1175/2009JCLI2514.1, 2009.

Singh, N., Mhawish, A., Ghosh, S., Banerjee, T., and Mall, R. K.: Attributing mortality from temperature extremes: A time series analysis in Varanasi, India, Science of The Total Environment, 665, 453–464, https://doi.org/https://doi.org/10.1016/j.scitotenv.2019.02.074, 2019.

Society, A. M.: On the Correlation of the Total Precipitable Water in a Vertical Column and Absolute Humidity at the Surface Author (s): E . E . Reber and J . R . Swope Published by : American Meteorological Society Stable URL : https://, 11, 1322–1325, 2022.

Steadman, R. G.: The Assessment of Sultriness. Part I: A Temperature-Humidity Index Based on Human Physiology and Clothing Science, J. Appl. Meteorol. Climatol., 18, 861–873, https://doi.org/10.1175/1520-0450(1979)018<0861:TAOSPI>2.0.CO;2, 1979.

https://doi.org/10.5194/essd-2026-103
Preprint. Discussion started: 1 April 2026
© Author(s) 2026. CC BY 4.0 License.

Stull, R.: Wet-bulb temperature from relative humidity and air temperature, J. Appl. Meteorol. Climatol., 50, 2267–2269, https://doi.org/10.1175/JAMC-D-11-0143.1, 2011.

Tian, H., Zhao, Y., Luo 罗明, M., He, Q., Han, Y., and Zhaoliang, Z.: Estimating PM2.5 from multisource data: A comparison of different machine learning models in the Pearl River Delta of China, Urban Clim., 35, 100740, https://doi.org/10.1016/j.uclim.2020.100740, 2021.

Tian, J., Zhang, Z., Zhao, T., Tao, H., and Zhu, B.: Warmer and wetter climate induced by the continual increase in atmospheric temperature and precipitable water vapor over the arid and semi–arid regions of Northwest China, J. Hydrol. Reg. Stud., 42, 101151, https://doi.org/10.1016/j.ejrh.2022.101151, 2022.

Utep, S., Tweedie, C., Lerma, L. O., Tweedie, C., and Kreinovich, V.: Increased Climate Variability Is More Visible Than Global Warming : A General System-Theory Explanation Increased Climate Variability Is More Visible Than Global Warming : A General System-Theory Explanation, 2014.

Vanos, J. K., Baldwin, J. W., Jay, O., and Ebi, K. L.: Simplicity lacks robustness when projecting heat-health outcomes in a changing climate, Nat. Commun., 11, https://doi.org/10.1038/s41467-020-19994-1, 2020.

Venugopal, V., Chinnadurai, J. S., Lucas, R. A. I., and Kjellstrom, T.: Occupational Heat Stress Profiles in Selected Workplaces in India, https://doi.org/10.3390/ijerph13010089, 2016.

Vicedo-Cabrera, A. M., Scovronick, N., Sera, F., Royé, D., Schneider, R., Tobias, A., Astrom, C., Guo, Y., Honda, Y., Hondula, D. M., Abrutzky, R., Tong, S., Coelho, M. de S. Z. S., Saldiva, P. H. N., Lavigne, E., Correa, P. M., Ortega, N. V., Kan, H., Osorio, S., Kyselý, J., Urban, A., Orru, H., Indermitte, E., Jaakkola, J. J. K., Ryti, N., Pascal, M., Schneider, A., Katsouyanni, K., Samoli, E., Mayvaneh, F., Entezari, A., Goodman, P., Zeka, A., Michelozzi, P., de'Donato, F., Hashizume, M., Alahmad, B., Diaz, M. H., Valencia, C. D. L. C., Overcenco, A., Houthuijs, D., Ameling, C., Rao, S., Di Ruscio, F., Carrasco-Escobar, G., Seposo, X., Silva, S., Madureira, J., Holobaca, I. H., Fratianni, S., Acquaotta, F., Kim, H., Lee, W., Iniguez, C., Forsberg, B., Ragettli, M. S., Guo, Y. L. L., Chen, B. Y., Li, S., Armstrong, B., Aleman, A., Zanobetti, A., Schwartz, J., Dang, T. N., Dung, D. V, Gillett, N., Haines, A., Mengel, M., Huber, V., and Gasparrini, A.: The burden of heat-related mortality attributable to recent human-induced climate change, Nat. Clim. Chang., 11, 492–500, https://doi.org/10.1038/s41558-021-01058-x, 2021.

Wang, J., Chen, Y., Tett, S. F. B., Yan, Z., Zhai, P., Feng, J., and Xia, J.: Anthropogenically-driven increases in the risks of summertime compound hot extremes, Nat. Commun., 11, 528, https://doi.org/10.1038/s41467-019-14233-8, 2020.

Wang, Y. and Wang, T.: Application of improved LightGBM model in blood glucose prediction, Applied Sciences, 10, 3227, https://doi.org/10.3390/app10093227, 2020.

Willett, K. M. and Sherwood, S.: Exceedance of heat index thresholds for 15 regions under a warming climate using the wet-bulb globe temperature, International Journal of Climatology, 32, 161–177, https://doi.org/10.1002/joc.2257, 2012.

Yamazaki, D., Ikeshima, D., Tawatari, R., Yamaguchi, T., O'Loughlin, F., Neal, J. C., Sampson, C. C., Kanae, S., and Bates, P. D.: A high-accuracy map of global terrain elevations, Geophys. Res. Lett., 44, 5844–5853, https://doi.org/10.1002/2017GL072874, 2017.

Yan, Y., Xu, Y., and Yue, S.: A high-spatial-resolution dataset of human thermal stress indices over South and East Asia, Sci. Data, 8, 229, https://doi.org/10.1038/s41597-021-01010-w, 2021.

https://doi.org/10.5194/essd-2026-103
Preprint. Discussion started: 1 April 2026
© Author(s) 2026. CC BY 4.0 License.

509 Zhang, R., Jia, X., and Qian, Q.: Analysis of lower-boundary climate factors contributing to the summer
510 heatwave frequency over eastern Europe using a machine-learning model, Atmospheric and Oceanic
511 Science Letters, 15, https://doi.org/10.1016/j.aosl.2022.100256, 2022a.

512 Zhang, T., Zhou, Y., Zhu, Z., Li, X., and Asrar, G. R.: A global seamless 1km resolution daily land
513 surface temperature dataset (2003-2020), Earth Syst. Sci. Data, 14, 651–664,
514 https://doi.org/10.5194/essd-14-651-2022, 2022b.

515 Zhang, X., Tang, Q., Zheng, J., and Ge, Q.: Warming/cooling effects of cropland greenness changes
516 during 1982–2006 in the North China Plain, Environmental Research Letters, 8, 24038,
517 https://doi.org/10.1088/1748-9326/8/2/024038, 2013.

518